 doi:10.20944/preprints202201.0143.v1

On the use of ^{210}Pb-based records of sedimentation rates and activity concentrations for tracking past environmental changes

J.M. Abril

Dpto. Física Aplicada I, ETSIA Universidad de Sevilla, Sevilla (Spain)
Carretera de Utrera km 1; D.P. 41013 Seville (Spain). Email: jmabril@us.es

Abstract

Lead-210 from natural atmospheric fallout is widely used in multidisciplinary studies to date recent sediments. Some of the ^{210}Pb-based dating models can produce historical records of sediment accumulation rates (SAR) and initial activity concentrations (A_0). The former have been profusely used to track past changes in the sedimentary conditions. Both physical magnitudes are differently affected by model errors (those arising for the partial or null accomplishment of some model assumptions). This work is aimed at assessing the effects on SAR and A_0 of model errors in the CRS, CS, PLUM and TERESA dating models, due to random variability in ^{210}Pb fluxes, which is a usual sedimentary condition. Synthetic cores are used as virtual laboratories for this goal. Independently of the model choice, SARs are largely affected by model errors, resulting in some large and spurious deviations from the true values. This questions their general use for tracking past environmental changes. A_0 are less sensitive to model errors and their trends of change with time may reflect real changes in sedimentary conditions, as it is shown with some real cores from varved sediments.

Keywords: ^{210}Pb dating; sedimentary conditions; model errors; initial activity concentrations; tracking environmental changes

Preprints (www.preprints.org) | NOT PEER-REVIEWED | Posted: 11 January 2022 doi:10.20944/preprints202201.0143.v1

1. Introduction

Radiometric dating was a revolutionary contribution to the study of sedimentary processes, since it is the only technique of general applicability allowing for an absolute age determination (Carroll and Lerche, 2003). In particular, the study of ^{210}Pb found in excess ($^{210}Pb_{exc}$ hereafter) with respect to its parent radionuclide (^{226}Ra) in sediment cores has been shown to provide useful information about the history of the sedimentary systems on a centennial time scale (Mabit et al., 2014). The method was first proposed for dating glacier ice (Goldberg, 1963) and was first applied to lacustrine sediments by Krishnaswamy et al. (1971), and to marine sediments by Koide et al. (1972).

^{222}Rn exhaled from the earth's surface into the atmosphere is dispersed and decays to ^{210}Pb, which is removed by precipitation and dry deposition. This ^{210}Pb fallout reaches the surficial sediments where it meets the ^{210}Pb produced by the in situ decay of ^{222}Rn (assumed in secular equilibrium with ^{226}Ra), and decays with a known half-life (22.3 a).

After coring and sectioning the sediment, mass activity concentrations of ^{210}Pb and ^{226}Ra can be measured for each slice, and $^{210}Pb_{exc}$ is routinely estimated as their difference on a layer-by-layer basis. When ^{226}Ra concentrations are largely irregular, the use of a model accounting for ^{222}Rn diffusion in the saturated porous media is advisable for estimating the supported ^{210}Pb (e.g., see Appelby, 1998). The mass depth scale, m, the dry mass per unit area accumulated from the sediment-water interface (SWI), remains invariant under natural compaction and sediment shortening (during coring, storage, and extrusion processes). The physical fundamentals for the mass-conservation of a particle-bound radioactive tracer in porous and accreting sediments with early compaction are relatively well understood (Abril, 2003). Nevertheless, a $^{210}Pb_{exc}$ vs. mass depth profile, $A(m)$, is unable to provide a chronology without the introduction of a series of assumptions on the fluxes of matter and activities reaching the SWI and on the involved post-depositional processes. Any set of assumptions which enables the construction of a chronology from $A(m)$ is known as a radiometric dating model.

A summary of the best-known ^{210}Pb-based dating models can be found, among others, in Mabit et al. (2014) or in Arias-Ortiz et al. (2018). As a brief update, it is worth mentioning the critical revision of the SIT model (Abril, 2015), the Bayesian formulation of the 'constant flux' model, by Aquino-López et al. (2018), known as the PLUM model, and the multimodal version of the TERESA model (Abril, 2020).

Although establishing a chronology is the primary interest of these models, some of them are able to provide historical series of sediment accumulation rates (SARs), so they have been widely used to track major past environmental changes. A search in SCOPUS with the criteria "^{210}Pb AND sediment" yields 5139 items, of which 2831 fit the search criteria "^{210}Pb AND sedimentation rate". As examples, abrupt or smooth changes in ^{210}Pb-derived SARs have often been related to waterworks, changes in land use, and to a wide variety of other anthropogenic activities that impact the aquatic environments, including global warming (e.g., Lu and Matsumoto, 2005; Madsen et al., 2007; Trabelsi et al., 2012; Begy et al., 2018; Chen et al., 2019). The ^{210}Pb-based models that allow for decoding of SAR records are: CRS (constant rate of supply; Appleby and Oldfield, 1978); CIC (constant activity concentration; Robbins, 1978); PLUM (Aquíno-López et al., 2018); SIT (sediment isotope tomography; Carroll and Lerche, 2003); TERESA (time estimates from random entries of sediments and activities, Abril, 2016; 2020). A summary of these models, including the CS (constant SAR) model, is presented in Annex A, where some references to specific software are also provided.

A practical and well-known limitation in the use of SARs is the large propagated errors involved in their estimation. This can be at least partially surpassed by using more accurate

Preprints (www.preprints.org) | NOT PEER-REVIEWED | Posted: 11 January 2022 doi:10.20944/preprints202201.0143.v1

analytical procedures and model approaches. Nevertheless, there is a more fundamental concern arising from the non-quantifiable model errors, and this is the focus of the present work.

Model errors in ^{210}Pb-based chronologies are the discrepancies among the model-predicted and the true values of ages due to the partial or null accomplishment of the model assumptions. They can be assessed with synthetic cores and varved sediments for which an independent chronology is available (Abril, 2019; 2020).

The choice of the model must be supported by our best understanding of how the flows of matter and $^{210}Pb_{exc}$ behave in the aquatic sedimentary environment studied. Based on a wide and systematic survey on laminated sediments from marine, riverine and lacustrine environments, Abril and Brunskill (2014) found that $^{210}Pb_{exc}$ fluxes onto the SWI (ϕ) and SARs largely varied over time, while both magnitudes were statistically correlated. These authors also found a large variation in initial $^{210}Pb_{exc}$ activity concentrations at the SWI, A_0, but they were uncorrelated with SARs. It could be thought that the temporal variability of ϕ automatically discards the application of the PLUM, CF-CS (constant flux with constant sedimentation) and CRS models, since they assume a constant flux. Nevertheless, an analysis of the properties of model errors has shown that the CRS chronologies can be acceptable for varying rates of supply when such variations are randomly distributed in the time-line (Abril, 2019). This random variability in fluxes is expected to occur in relatively unperturbed and low-energetic aquatic environments, and it would be linked to short-term climatic variability. Thus, the many application cases of the CRS model where chronologies have been validated against independent chronostratigraphic markers are not in contradiction with the empirical evidence shown by Abril and Brunskill (2014) of widespread conditions of varying fluxes.

The above statements can be better understood with the example shown in Fig. 1. It plots the $^{210}Pb_{exc}$ vs. mass depth profile for a varved sediment core sampled in 1999 in the Pettaquamscutt River basin (data from Lima et al., 2005a). The application of the CRS model (which assumes a constant $^{210}Pb_{exc}$ flux) leads to the chronology plotted in the secondary axis; and it adequately matches the ^{137}Cs time-mark (the 1963 maximum in bomb fallout). In absence of varves, the above model chronology, supported by an independent chronostratigraphic mark, fulfil the commonly accepted requirements for its validation (Smith, 2001).

The varve chronology allows decoding from the empirical $^{210}Pb_{exc}$ profile the historical records of $^{210}Pb_{exc}$ fluxes onto the SWI (e.g., see Abril and Brunskill, 2014). They are plotted in the lower panel of Fig. 1. Fluxes show a large temporal variability (with the time resolution of the slicing), violating the main assumption of the CRS model. Nevertheless, as in this case such variability is overall randomly distributed in the time line, model errors lead to positive and negative deviations in model ages that tend to compensate mutually. Thus, the model chronology, when compared with that from varves, shows a close agreement but for the older layers. Discrepancies for these latter are partially contributed by the model sensitivity to accurate estimations of the total inventory and by non-random fluctuations in $^{210}Pb_{exc}$ fluxes in the older dates (Fig. 1).

However, the above discrepancies in model-ages are not the focus of the present work, since they have been previously studied (Abril, 2019; 2020). In particular, when changes in environmental conditions lead to a stepped shift on the mean value of ϕ, over which a random variability is superposed; the piecewise version of the models CF-CS, CRS, CIC and TERESA has shown good performance (Abril, 2019; 2020). When changes in environmental conditions lead to a continuous trend of increase/decrease in ϕ, classical models failed; however the Multimodal TERESA model has shown promising results (Abril, 2020).

Preprints (www.preprints.org) | NOT PEER-REVIEWED | Posted: 11 January 2022 doi:10.20944/preprints202201.0143.v1

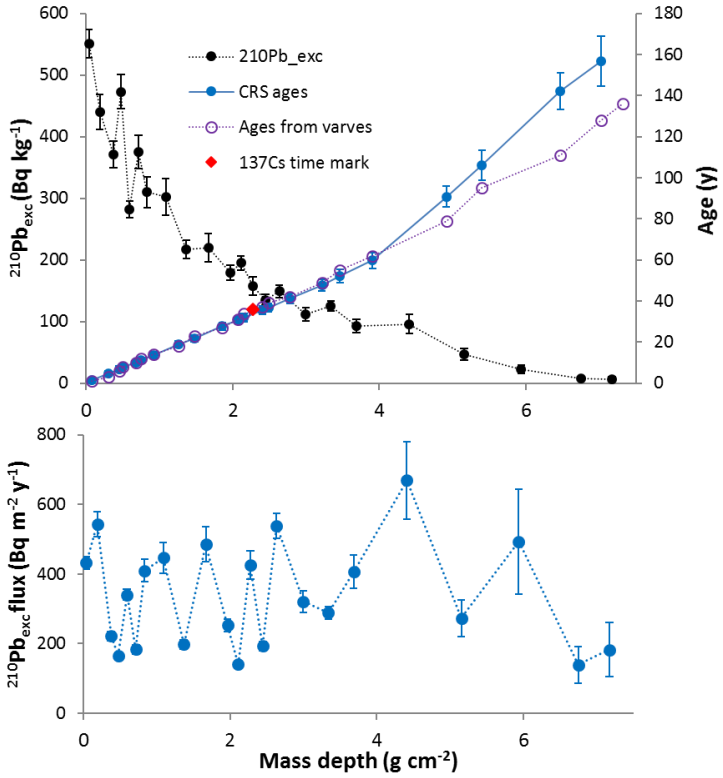

Figure 1: $^{210}Pb_{exc}$ vs. mass depth profile for a varved sediment core from the Pettaquamscutt River (raw data from Lima et al., 2005a). The CRS chronology is plotted on the secondary axis and compared against the 1963 time-mark from ^{137}Cs and the chronology from varves. This last allowed for the reconstruction of the $^{210}Pb_{exc}$ paleofluxes plotted in the lower panel.

Here we are concerned with studying how model errors can differently affect the estimation of SARs and A_0; and what are the potential limitations for their use in tracking past changes in sedimentary conditions. Although they are not a priori quantifiable, model errors are always present in real cases. This paper will show that because of the mathematics involved in the estimation of SARs from a model chronology, model errors lead to spurious and so large deviations from the true values that pose into question any attempt of using SARs for tracking past environmental changes. Nevertheless, this work will prove that A_0 are less sensitive to model errors, so that they meet the conditions for their use in the study of past changes in sedimentary conditions, as it will be shown with synthetic cores and real varved-sediments.

Here we will be consider models allowing for the estimation of time series of SARs and A_0, namely the CRS, CS, CIC, PLUM, SIT and TERESA models. They share three assumptions: i) continuity of the sequence (i.e., there is no missing layers by erosion, neither major episodic depositional-events); ii) $^{210}Pb_{exc}$ behaves as a particle-associated tracer, and new inputs are deposited at the SWI over the previously existing material; iii) there is no post-depositional redistribution. An additional assumption is needed for deriving the chronology, and this is specific to each model, as briefly reviewed in Annex A.

It is worth noting that the present concern is the effect of model errors in those situations where the model chronology can be globally acceptable for its final use (such as for the last century interval in the example of Fig. 1). Acceptability may rely on independent chronostratigraphic markers (e.g., tephras, bomb fallout radionuclides, etc.), internal consistency tests (equivalent constant fluxes pre and postdating a reference date, jump and slope discontinuities in a cluster analysis –see Abril, 2019) and the holistic analysis of the available data for the studied core. Not considered here are those cases with non-proper applications of

Preprints (www.preprints.org) | NOT PEER-REVIEWED | Posted: 11 January 2022 doi:10.20944/preprints202201.0143.v1

the above models that lead to erroneous chronologies and to unreliable records of SARs and A_0, such in cases with relevant non-ideal deposition (Abril and Gharbi, 2012), mixing (Robbins and Edgington, 1975; Abril et al 1992; Abril 2004), diffusion (Laissaoui et al., 2008), or continuous trends of change in fluxes (Abril, 2019; 2020).

2. Methods

In this study the mass depth scale, *m*, is adopted. The mass sedimentation rate, SAR, is represented by the symbol *w*. The model assumption ii) can be summarized as ideal deposition conditions and mathematically expressed as:

$$\phi = wA_0, \tag{1}$$

where A_0 is the mass activity concentration of $^{210}Pb_{exc}$ in the sediment layer under formation at the SWI.

In practice, the definition of the physical magnitudes must be adapted to account for the finite resolution of the slicing. The sketch in Fig. 2 will serve to illustrate the effect of the model errors in the estimation of SARs and initial activity concentrations. It shows a certain slice in a sediment core, labelled with index *i*, and for which its mass thickness per unit area, Δm_i, and $^{210}Pb_{exc}$ mass activity concentration, A_i, have been determined and reported with their associated uncertainties. Note that A_i is a physically averaged value within each slice because of the homogenization of the sample material before radiometric measurements. The mass depth scale can be built by aggregating Δm_i.

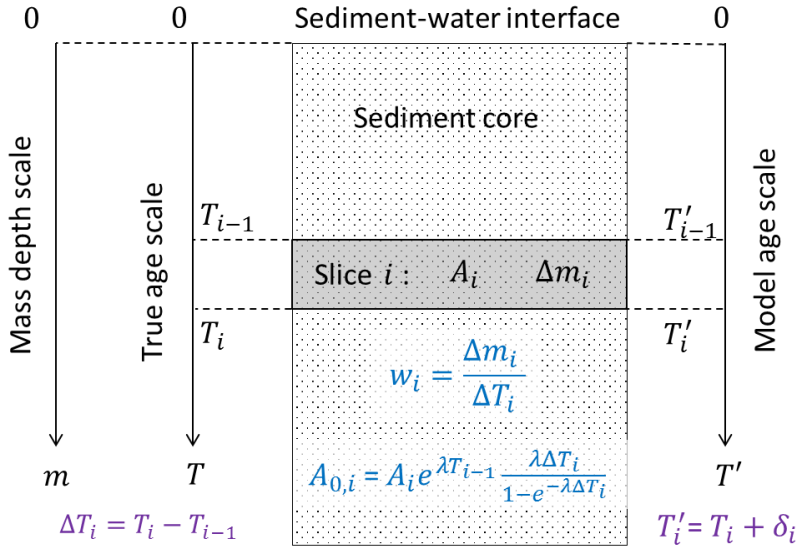

Figure 2: Sketch illustrating the true and model chronologies, the latter being affected by model errors (deviations arising from a non-proper accomplishment of the model assumptions). Also depicted are the physical magnitudes measured in a sediment slice (the mass thickness per unit area,Δm_i, and the $^{210}Pb_{exc}$ activity concentration, A_i), and those derived from the chronology (sedimentation rates, w_i, and initial activity concentrations, $A_{0,i}$).

Let us assume that a true chronology, $T(m)$, is known for the core (e.g. a varve chronology). The true time interval bounding the slice *i* is $\Delta T_i = T_i - T_{i-1}$, and the mean value of the mass sedimentation rate for this slice is:

$$w_i = \frac{\Delta m_i}{\Delta T_i}. \tag{2}$$

Preprints (www.preprints.org) | NOT PEER-REVIEWED | Posted: 11 January 2022 doi:10.20944/preprints202201.0143.v1

The $^{210}Pb_{exc}$ inventory in the slice is $A_i \Delta m_i$, and it can be seen as the cumulative result, after radioactive decay, of an equivalent constant flux $\phi_{e,i}$ lasting from T_{i-1} until T_i:

$$A_i \Delta m_i = \int_{T_{i-1}}^{T_i} \phi_{e,i} e^{-\lambda t} dt.$$

Solving for $\phi_{e,i}$ and taking into account Eq. (2):

$$\phi_{e,i} = w_i A_i e^{\lambda T_{i-1}} \frac{\lambda \Delta T_i}{1-e^{-\lambda \Delta T_i}} \quad (3)$$

The mean value of the initial activity concentration for slice *i* can be estimated from Eq. 3 assuming w_i being constant during the time interval ΔT_i:

$$A_{0,i} = A_i e^{\lambda T_{i-1}} \frac{\lambda \Delta T_i}{1-e^{-\lambda \Delta T_i}} \quad (4)$$

In the common case of $\lambda \Delta T_i \ll 1$ the above expression can be approached as:

$$A_{0,i} \cong A_i e^{\lambda (T_{i-1} + \Delta T_i/2)} \quad (5)$$

Let us now consider that by using a ^{210}Pb-based dating model the chronology $T'(m)$ has been built. At least conceptually, one can consider that it is possible to achieve very small analytical uncertainties (e.g., with high-precision instruments, large counting times and repeated measurements). Despite this, at any sediment horizon of mass depth m_i, the two chronologies, $T(m)$ and $T'(m)$, will differ by a certain amount because the partial accomplishment of the model assumptions, so that $T_i' = T_i + \delta_i$. The amount δ_i is the model error, and it can take positive or negative values. A detailed study of the model errors for the case of the CRS model can be found in Abril (2019), where δ_i is estimated for any arbitrary fluctuations around a baseline value of the $^{210}Pb_{exc}$ flux onto the SWI. The role of model errors in the CIC and CF-CS models is discussed in Abril (2020).

In this work, model errors will be assessed using synthetic cores and varved sediments but at this point, an estimate of the order of magnitude of δ_i can be done as follows. Abril and Brunskill (2014) found that about 1/3 of the $\phi_{e,i}$ values had relative deviations from their arithmetic mean in the core greater than 25 %. They used a first-order estimate for δ_i, which resulted to be a function of ΔT_i. According to their estimates, values of $\delta_i \gtrsim 2$ a can be expected for 1/3 of the cases, and larger deviations are possible but less frequent.

A model chronology can be considered globally acceptable when the absolute deviation remains below a certain limit, ε, and the deviations are not systematic. Depending on the final use of the data, values of 5-10 a for ε could be reasonable. The above is a particular choice for the acceptability criterion, and other formulations based on relative uncertainties are equally possible.

The SAR value estimated from the model-chronology is (after Eq. 2):

$$w_i' = \frac{\Delta m_i}{\Delta T_i + (\delta_i - \delta_{i-1})} = w_i \frac{1}{1 + (\delta_i - \delta_{i-1})/\Delta T_i}. \quad (6)$$

Note that δ_i are algebraic deviations and they do not follow the squared composition rule, unlike the propagated errors with their associated Normal probability distributions (e.g., Bevington and Robinson, 2003). According to the above figures, the term $(\delta_i - \delta_{i-1})/\Delta T_i$ in some cases can take values close to -1, resulting in large deviations of the model SARs with respect to the true values. Thus, it is possible to find in the record of model SARs some spurious extreme values that are not linked to any environmental change.

The estimation of the initial activity concentration from the model chronology is (after Eq. 5)

$$A_{0,i}' = A_i \, e^{\lambda \frac{\delta_i + \delta_{i-1}}{2}}. \quad (7)$$

Preprints (www.preprints.org) | NOT PEER-REVIEWED | Posted: 11 January 2022 doi:10.20944/preprints202201.0143.v1

Here the correcting factor is always less than $e^{\lambda\varepsilon}$. Thus, for $\varepsilon = 10$, the maximum deviation is less than 36%. This makes the records of $A'_{0,i}$ more suitable for tracking past environmental changes.

In practical cases, the true chronology remains unknown and the measured magnitudes are informed with non-negligible uncertainties, which propagate to the model-estimated magnitudes (ages, SARs and initial activity concentrations). Although non-quantifiable, the model errors are still present and their effects prevail as above estimated. It is worth noting that the particular model assumptions can allow for alternative estimates for SAR and initial activity concentrations, which affects to the propagated uncertainties, but their values must be necessarily equivalent to those from Eqs. 6 and 7 because of the internal consistence of the chronology, so they are equally affected by model errors.

Model errors and the use of Eqs. 6 and 7 will be first assessed with a synthetic core generated with random and independent temporal variability in SAR and A_0. This violates the model assumptions of a constant flux or a constant initial activity concentration. The source of model errors for TERESA is discussed further below. To generate the synthetic core, we have adopted the methodology described by Abril (2016; 2020).

The use of $A'_{0,i}$ records for tracking past environmental changes will be further demonstrated with a set of varve sediments from the scientific literature for which suitable datasets exist.

The basic equations of the studied models are presented in Annex A, and they have been implemented with software developed for this work under Excel and BASIC environments, with the support of some MATLAB tools.

3. Results

3.1. Synthetic core SC-1

A synthetic core has been generated following the methodology described by Abril (2016). It contains 30 slices of 1 cm thick each. A realistic bulk density profile has been built with early compaction, involving white noise, a scaling factor of 0.4 cm^{-1}, and bulk density values at SWI and at large depths of ρ_0 = 0.2 g cm^{-3} and ρ_∞=0.65 g cm^{-3}, respectively. Initial activities and SARs have been assigned to each slice using randomly sorted values following normal distributions with mean values of 300 Bq kg^{-1} and 0.15 g $cm^{-2}a^{-1}$, and relative deviations of 0.25 and 0.30, respectively. This leads to fluxes onto the SWI with random variations and randomly distributed in the time-line. The true chronology is inferred from SARs and mass thickness; this last is estimated from the bulk density and the 1 cm depth interval of the slices. The chronology is then used to correct for radioactive decay the initial activity concentrations to simulate this way the empirical values of the $^{210}Pb_{exc}$ activity concentrations. Uncertainties of 10% have been arbitrarily ascribed to support further discussion (they are typical values for measurements by alpha spectrometry; e.g., see, Zaborska et al., 2007). This synthetic profile is shown in Fig. 3.

CRS model

The CRS model (see Annex A) has been applied to this synthetic core. This involved the usual correction for the total inventory based upon the extrapolation of the exponential trend prevailing at the deepest portion of the core (the reference-SAR method – see Appleby, 2001). The results are shown in Fig. 3.

Preprints (www.preprints.org) | NOT PEER-REVIEWED | Posted: 11 January 2022 doi:10.20944/preprints202201.0143.v1

Despite the fact that the synthetic $^{210}Pb_{exc}$ fluxes onto the SWI were not constant over time (mean and standard deviation of 462 and 220 Bq $m^{-2}a^{-1}$, respectively), the CRS ages reasonably fitted the true chronology (Fig. 3, first panel). The small synthetic analytical uncertainties used in this exercise serve to unambiguously interpret deviations from the true chronology as the expression of model errors. These are due to the non-proper accomplishment of the model's assumption of a constant flux. The temporal variability in fluxes is large, but randomly sorted in time, so that positive and negative deviations in the chronology tend to mutually compensate.

The maximum absolute deviation in chronologies is 9.4 a. The ratio $(\delta_i - \delta_{i-1})/\Delta T_i$ takes values in the range -0.55 to 2.20 so that in Eq. 6 true SARs are multiplied by a factor ranging from 0.31 to 2.20. This leads to large and spurious deviations in the model-SARs with respect to the true (synthetic) values, as shown in Fig. 3, second panel. It is worth noting that such deviations are not a consequence of using Eq. 2, but of the model architecture itself. Indeed, CRS-SARs (and their propagated uncertainties) have been estimated from Eq. A-3 (note that the ratio $\frac{A(m)\Delta m}{\Sigma_m}$ ranged from 0.05 to 0.31, allowing for the first-order approach –see Annex A). As seen in Fig. 3, and despite the relatively small propagated errors, the model-SAR records are of little use for interpreting past environmental changes.

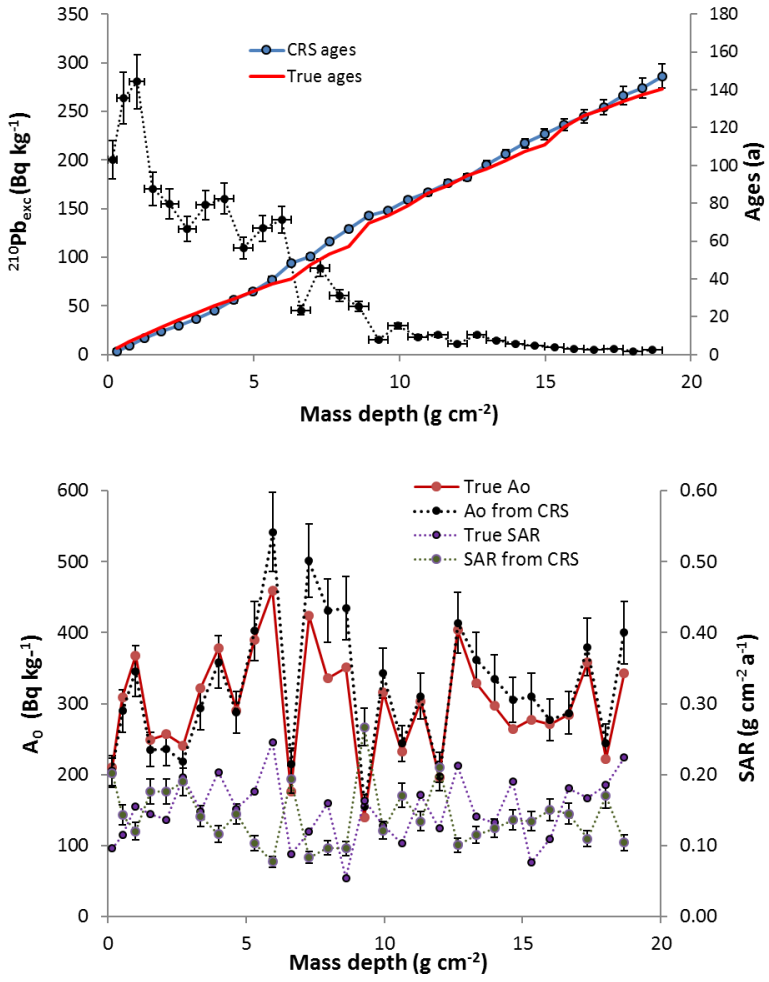

Figure 3. Synthetic profile of $^{210}Pb_{exc}$ versus mass depth (m) (first panel) generated with initial activity concentrations of $^{210}Pb_{exc}$ and SARs with a random variability (second panel – see text for details). The CRS model has been applied to decode the chronology (first panel) and the records of initial activity

Preprints (www.preprints.org) | NOT PEER-REVIEWED | Posted: 11 January 2022 doi:10.20944/preprints202201.0143.v1

concentrations and SARs (second panel), where they are compared with the corresponding true (synthetic) values. CRS SARs have been estimated from Eq. A-3. The error bars are 1σ propagated errors.

The term $\frac{\delta_i+\delta_{i-1}}{2}$ in Eq. 7 ranged from -3.1 to 8.1 a, so $e^{\lambda\frac{\delta_i+\delta_{i-1}}{2}}$ ranged from 0.91 to 1.28. In this way, the deviations of the CRS initial activity concentrations with respect to the synthetic values remained reasonably constrained (Fig. 3) so that their records can be useful for decoding past environmental changes.

PLUM model

The PyPlum version for Python (see Annex A) has been applied to the synthetic core SC-1. The closest agreement to the true chronology was achieved by using a value of 0.01 for the parameter *Al*, which is involved in the definition of a chronological limit (Aquino-López et al., 2018). The results are shown in Fig. 4 where the PLUM ages are bounded by their 95% confidence interval.

Despite the fact that the $^{210}Pb_{exc}$ flux is not constant over time, the PLUM chronology runs close to the true (synthetic) one, with the exception of the oldest layers. By excluding the four deepest slices, the maximum absolute deviation of the chronology is 10.9 a. The ratio $(\delta_i - \delta_{i-1})/\Delta T_i$ takes value in the range -0.52 to 1.85 so that in Eq. 6 true SARs are multiplied by a factor ranging from 0.35 to 2.10, similar to those found for the CRS model. The term $e^{\lambda\frac{\delta_i+\delta_{i-1}}{2}}$ in Eq. 7 ranged from 0.88 to 1.38 (see Fig. 4), giving some chance for using the model $A'_{0,i}$values for tracking past environmental changes.

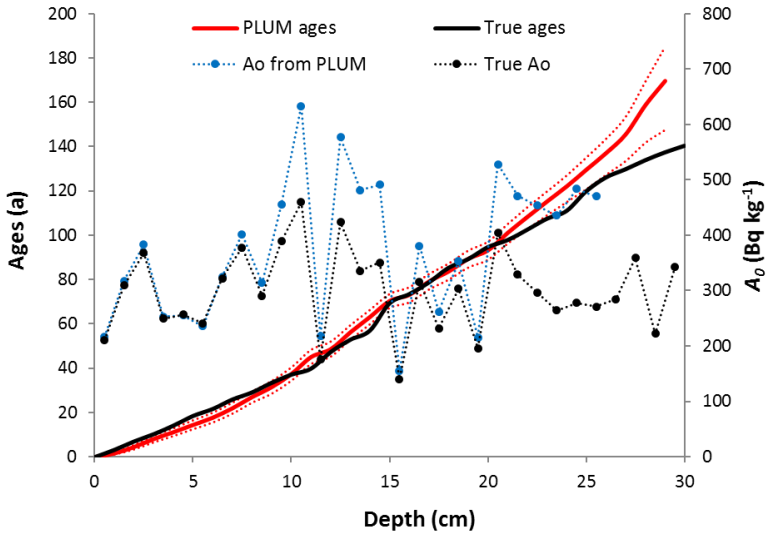

Figure 4. Chronology produced by the PLUM model for the synthetic core SC-1 (see text and Fig. 2) compared with the true (synthetic) ages. Model ages are bounded by the 95% confidence interval (dot lines). The initial activity concentrations derived from the above chronology are depicted on the secondary axis along with the synthetic ones.

TERESA model

The TERESA model has been applied to the synthetic core SC-1. Results are shown in Fig. 5. The chronology closely matches the synthetic one, but it is affected by model errors. Indeed, the model reencounters the $\bar{w}$, $\bar{A}_0$, s_w and s_A values used for the synthetic core, but as it uses a different arrangement of the pairs of normal-typified values ($z_{1,i}$, $z_{2,i}$), the model-distributions

Preprints (www.preprints.org) | NOT PEER-REVIEWED | Posted: 11 January 2022 doi:10.20944/preprints202201.0143.v1

for SARs and $A'_{0,i}$ are only a proxy to the true (synthetic) ones (see a more detailed discussion in Annex A).

The maximum deviation in the chronology is 7.2 a. The initial activity concentrations estimated by TERESA closely fit the synthetic ones (Fig. 5, panel 1). The SAR values of TERESA and the synthetic ones are well criss-crossed, but with some spurious excursions out of the trend (Fig. 5, panel 2).

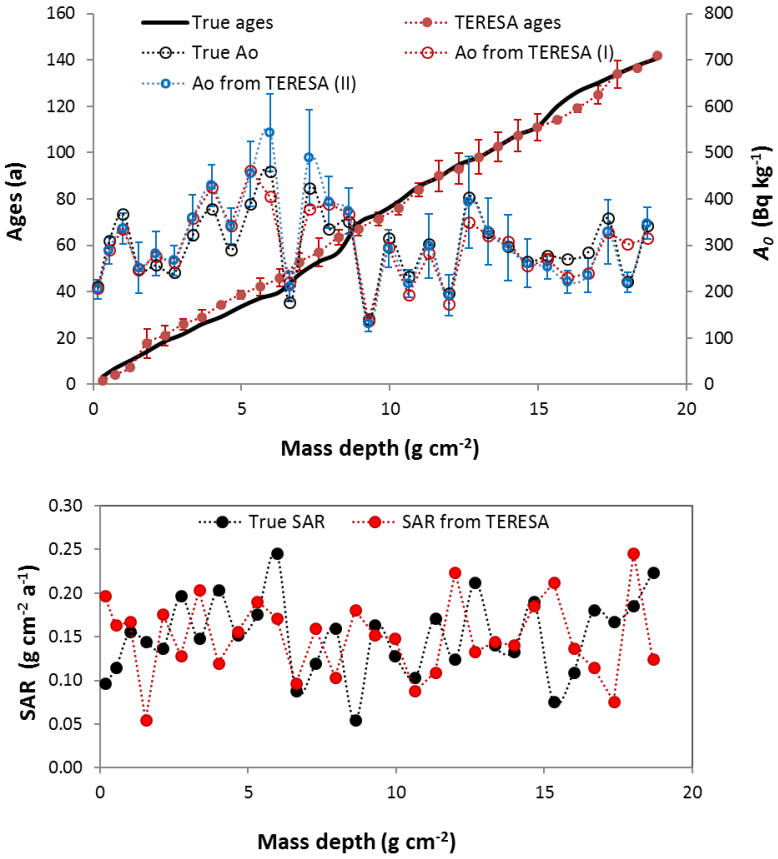

Figure 5. First panel: Chronology produced by the TERESA model for the synthetic core SC-1 (see text and Fig. 2) compared with the true (synthetic) ages. The initial activity concentrations derived from the above chronology are depicted on the secondary axis along with the synthetic ones. (I) refers to the sorting of pairs (w_i, $A_{0,i}$), and (II) applies Eq. 7. The error bars are 1σ propagated errors. Second panel: Comparison of SAR values estimated from TERESA and synthetic ones.

CS model

The constant-sedimentation model can be built from a known reference date. In the synthetic core, the sediment horizon at mass depth 8.28 g cm^{-2} has a synthetic age of 57.2 a. It has been used as a known time marker to estimate a SAR value of 0.145 ± 0.003 g cm^{-2}a^{-1}, allowing for the construction of the chronology shown in Fig. 6. In this example, the CS model provides a good proxy to the true chronology for ages postdating the time mark, but the chronology shows a systematic displacement for older ages. It is possible to estimate initial activity concentrations by Eq. 7 using the CS chronology. Results are shown in Fig. 6 (secondary axis). They match the true values postdating the reference date. For older ages, the model values $A'_{0,i}$ show a systematic deviation from the true ones but they track their changes over time.

Preprints (www.preprints.org) | NOT PEER-REVIEWED | Posted: 11 January 2022 doi:10.20944/preprints202201.0143.v1

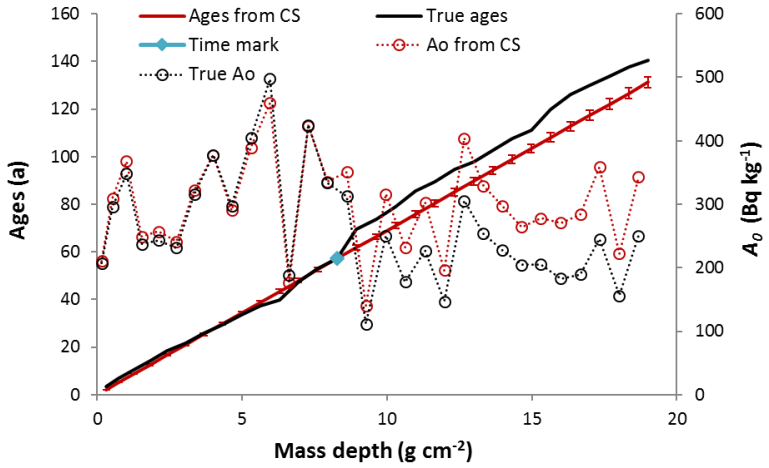

Figure 6. Chronology produced by the CS model for the synthetic core SC-1 using a known time mark. The error bars are 1σ propagated errors. It is compared with the true (synthetic) ages. The initial activity concentrations derived from the above chronology are depicted on the secondary axis along with the synthetic ones.

Model intercomparison

From the above results with the synthetic core SC-1, the CRS and TERESA models produced the most reliable estimates for the chronology and the initial activity concentrations. The PLUM model shares the assumptions of the CRS model, except for the assumption of a steady-state total inventory. Therefore, in those cases where this last assumption is not under question, or its use is not seriously limited by a partial recovery of the total inventory, the PLUM and CRS chronologies should be mutually consistent (as shown in Aquino-López et al., 2018). Thus, for subsequent analyses in this work, the CRS model has been preferentially applied instead of the PLUM model. Reasons are the spread use of the former and its mathematical simplicity. The CS model built from the available time marks usually lacks any independent validation, and the chronology for the portion of the core below the oldest reference date is not reliable enough. Nevertheless, this model is simple to use and can provide a valuable first level of understanding.

3.2. Varved sediment core VC-1

Core VC-1 is a varved sediment sampled in April 1999 in the Pettaquamscutt River basin (Rhode Island, Northeast USA) at 41º30' N, 71º26'W, and 19.5 m depth (data from Lima et al., 2005a). It has been previously presented in Fig. 1. Varves were defined by biogenic and clastic layers. Raw data can be seen in the original reference and in the supplementary material of Abril (2020). In this last reference, $^{210}Pb_{exc}$ paleofluxes, initial activity concentrations and SAR records were reconstructed from the varve chronology. $^{210}Pb_{exc}$ paleofluxes showed a large temporal variability that was randomly sorted along the time line (see Fig.1, lower panel). The CRS, CF-CS, CIC and TERESA models were applied to this core (Fig.1 in this work and Abril, 2020). The resulting chronologies and SAR records are presented in the above reference. All of the models produced a similar output: a reasonable proxy to the true chronology and to the mean values of fluxes and SARs.

The present goal is to compare the predictions for initial activity concentrations from the CRS and TERESA models. The 1963 ^{137}Cs peak (25 ± 2 Bq·kg^{-1}) appears in the sediment slice of 17.75-18.75 cm (Lima et al., 2005a), which allows an independent estimate for the

Preprints (www.preprints.org) | NOT PEER-REVIEWED | Posted: 11 January 2022 doi:10.20944/preprints202201.0143.v1

mean SAR of 0.063 ± 0.004 g $cm^{-2}a^{-1}$. This value has been used here for building a CS-chronology from which initial activity concentrations were then estimated by Eq. 7. The results are shown in Fig. 7. As seen in this figure, the three models were able to reasonably reproduce the temporal variability of the initial activity concentration inferred from the varve chronology, although the CS model provides a poorer description for the older layers.

3.3. Varved sediment core VC-2

Core VC-2 was sampled in 1971 in Santa Barbara Basin, at geographical coordinates 34º14.0'N, 120º01.5'W and 575 m water depth. It is a varved sediment with annual designations based on a direct correlation of sediment thickness and rainfall for the past 100 years (data from Koide et al., 1972, 1973). Raw data can be seen in the original reference and in the supplementary material of Abril (2020). In this last reference, $^{210}Pb_{exc}$ paleofluxes, initial activity concentrations, and SAR records were reconstructed from the varve chronology. $^{210}Pb_{exc}$ paleofluxes showed random variations from 1930 to 1960, followed by a continuous trend of increase that peaked around 1970, shortly before the coring. The increase in fluxes was mostly contributed by an increase in SAR. This continuous trend of change in fluxes leads to the failure of the CF-CS, CIC, and CRS models, as discussed in Abril (2016, 2019).

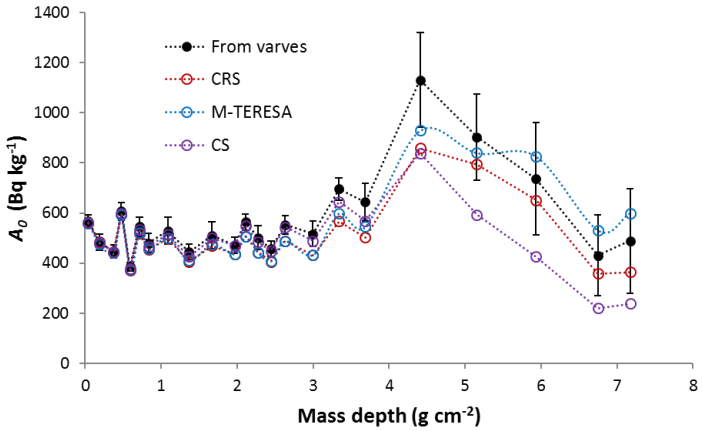

Figure 7. Initial activity concentrations estimated from the CRS, FM-TERESA, and CS models for core VC-1, a varved sediment core from the Pettaquamscutt River (raw data from Lima et al., 2005a). Also depicted are the initial activity concentrations estimated by Eq. 7 from the varve chronology, along with their propagated errors.

The TERESA model was able to provide a reliable chronology for this core as shwon in Abril (2016). Figure 8 shows the records of SARs and the $^{210}Pb_{exc}$ initial activity concentrations computed from TERESA, and they are compared against the corresponding values estimated from the varve chronology. Although SARs from TERESA are well criss-crossed with those from varves, there are some spurious excursions out of the trend. The initial activity concentrations estimated by TERESA closely fit the ones from varves, as seen in Fig. 8.

3.4 Varved sediment core VC-3

Data for core VC-3 are available in the supplementary material from the work by Tylmann et al. (2016). The sediment core was collected in September 2011 in Lake Zabinskie at 54º07'54.50''N, 21º59'01.1''E, and 44.4 m water depth. The core showed biogenic varves.

Preprints (www.preprints.org) | NOT PEER-REVIEWED | Posted: 11 January 2022 doi:10.20944/preprints202201.0143.v1

Abril (2020) presented the $^{210}Pb_{exc}$ paleofluxes, initial activity concentrations, and SAR records as decoded from the varve chronology. $^{210}Pb_{exc}$ paleofluxes showed a non-random variability over time with an overall trend of decrease.

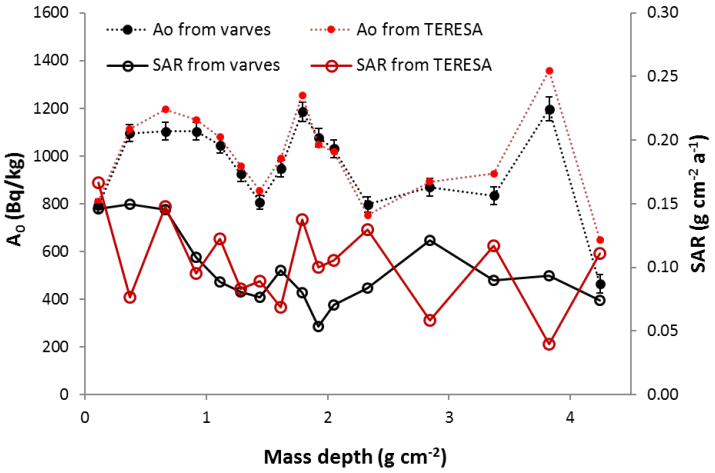

Figure 8. SAR and $^{210}Pb_{exc}$ initial activity concentrations estimated from the TERESA model for core VC-2, a varved sediment core from the Santa Barbara Basin (raw data from Koide et al., 1972; 1973). Also depicted are the SAR and initial activity concentrations estimated from the varve chronology, the latest informed with their 1σ propagated errors.

The cluster analysis allowed the definition of three clusters, and the piecewise versions of the CF-CS and CRS models were successfully applied. The new fast-multimodal version of the TERESA model (FM-TERESA) was also applied to this core (Abril, 2020). The piecewise version of the CF-CS model allowed for capturing the mean values of SAR and A_0 in each transect (or cluster). This provides a first level of insight into their temporal variability. The present goals focus on the piecewise version of the CRS and the FM-TERESA models, particularly in their estimates for the historical records of SARs and initial activity concentrations. It is worth noting that in the present work the piecewise version of the CRS model does not use any external time marker (such as ^{137}Cs peaks) but the ages (as estimated from CF-CS) of the true (jump and/or slope) discontinuities observed in the log-plot of $A(m)$ (see Abril, 2020).

The chronologies produced by the piecewise CRS and the FM-TERESA models have been presented elsewhere (Abril, 2020), and they were in reasonable close agreement with the one from varves. The records of SARs and initial activity concentrations estimated from these models are shown in Fig. 9. Again, the initial activity concentrations computed by both models closely follow the complex variability observed in the true values (from varves), while SARs values fail to do so. Particularly, both models show large discrepancies in SARs in the first transect (0-6 g cm^{-2}). Varve SARs show a pronounced peak that can be interpreted as a period of continuous increase followed by another period of continuous decrease. These continuous trends of change can separately produce the failure of these models, but in this case, positive and negative deviations mutually compensate along the transect. A more detailed discussion can be found in Abril (2020). Despite these large discrepancies in SARs, as shown in Fig. 9, the initial activity concentrations produced with both models remain reliable estimates of the true values.

Preprints (www.preprints.org) | NOT PEER-REVIEWED | Posted: 11 January 2022 doi:10.20944/preprints202201.0143.v1

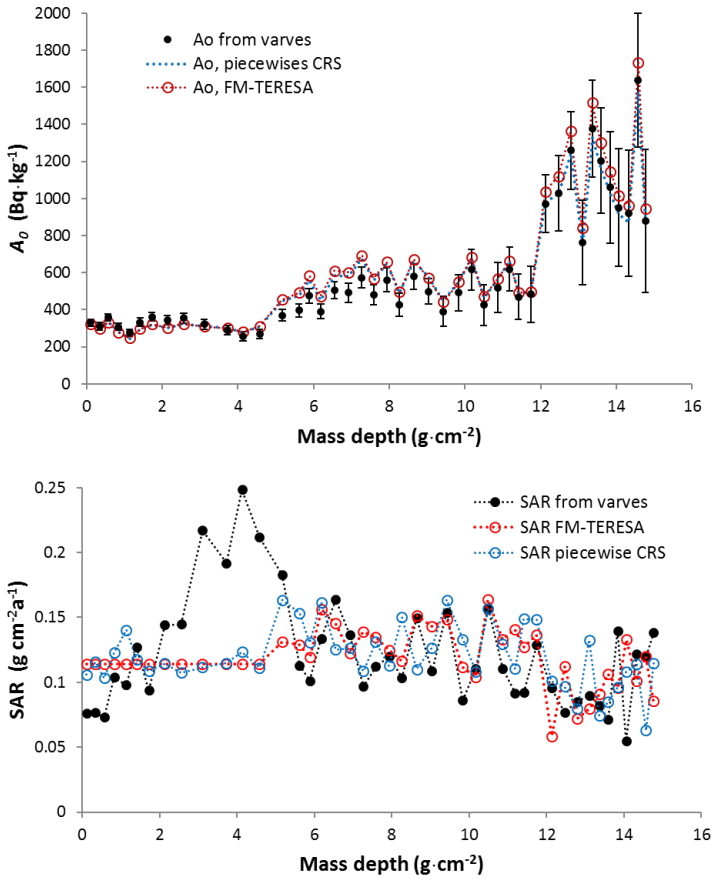

Figure 9. First panel: Initial activity concentrations computed by the piecewise-CRS and FM-TERESA models for the varved sediment core VC-3, compared with the corresponding values estimated from the varve chronology (shown with 1σ propagated errors). Second panel: Comparison of SAR values estimated from the above two models compared against the values estimated from the varve chronology.

4. Discussion

The results of this study have shown that ^{210}Pb-based SAR records are largely affected by the always present model errors. Consequently, they are of little use for tracking past changes in sedimentary conditions. On the contrary, the initial activity concentrations, which had received little attention up to date, are less sensitive to model errors, and their trends of change with time may reflect real changes in environmental conditions. Furthermore, their propagated uncertainties are smaller than those for SARs. However, while changes in SAR are quite straightforward to interpret (increase or decrease of mass flow onto the SWI), this is not the case for A_0. In what follows we review a series of factors affecting this physical magnitude.

The slice-averaged value of A_0 is the aggregate result of mass flows with multiple provenances and varying intensities, involving a diversity of histories of $^{210}Pb_{exc}$ uptake, which are mediated by dynamically varying physic-chemical conditions and contact times, and by the mineralogy, size and topology of the particulate matter.

Particulate matter in natural aquatic environments has complex shapes with irregular and porous surfaces and free edges. This conforms the topological environment where different reaction sites are distributed for the uptake of the meteoric ^{210}Pb, now present in the aqueous phase. Theoretical considerations (Abril and Fraga, 1996; Abril 1998a; 1998b) and experimental studies (He and Walling, 1996) have shown a decrease of A_0 with particle size. The uptake kinetics is also relevant in dynamic situations where particulate matter has limited contact times

Preprints (www.preprints.org) | NOT PEER-REVIEWED | Posted: 11 January 2022 doi:10.20944/preprints202201.0143.v1

with the aqueous phase before settling, or when the concentration of the tracer in the aqueous solution undergoes rapid changes. Experimental studies (El-Mrabet et al., 2001; Barros and Abril, 2004) have shown that uptake kinetics can be described by a series of parallel or consecutive reactions with decreasing reversibility and with different characteristic times, ranging from minutes up to weeks. After settling, particulate matter can still capture meteoric ^{210}Pb from the aqueous solution, in a process governed by the molecular diffusion through the connected water pores and mediated by the fraction of the surface of theparticles that remains in physical contact with the aqueous phase (Barros et al., 2004).

The granulometric fingerprint of sediments can show a natural short-term variability, but it can also experience abrupt changes, among other factors, due to damming and other waterworks.

Evidence of particle-size effects on A_0 from field studies is not conclusive. Thus, Sun et al. (2018) found a strong positive correlation between the clay component (< 4 μm) and $^{210}Pb_{exc}$ in a wide set of sediment cores from the coastal area of the Yangtze River Estuary. Aalto and Nittrouer (2012) used clay-normalized ^{210}Pb activity concentrations to establish geochronologies of flood events in large tropical river systems. Other works have reported weak or negligible dependence of ^{137}Cs and $^{210}Pb_{exc}$ concentrations with particle grain sizes in the range of 4 μm up to 2000 μm. This is the case in the studies by Alonso Hernández et al. (2006) with coastal sediments in Cienfuegos Bay, and by Mantero et al. (2019), whit some estuarine sediments from Spain and Ghana. Thus, unlike under ideal experimental conditions, the complexity of real aquatic environments does not support rules of general use for the whole range of particle sizes and for any system studied.

The particulate matter reaching the SWI may have different provenances: i) from riverine, runoff, and aeolian transport from different sites in the catchment; ii) removed from transient sedimentation sites in the aquatic system; iii) biogenic production, etc. This particulate matter carries $^{210}Pb_{exc}$ that has been uptaken from atmospheric fallout at the sites of their provenances (surface soils, surficial transient sediments, etc.) or during its path through the water column, and these solids still can further uptake meteoric ^{210}Pb after settling at the core site. The empirical statistical correlation among fluxes and SARs reported by Abril and Bruskill (2014) indicates that the major contribution to $^{210}Pb_{exc}$ fluxes is generally the one already attached to the mass flows reaching the SWI. Short-term variability in climatic conditions can alter the global intensity of the mass flow reaching the SWI (a change in SAR), but this also modifies the partial contribution of different provenances and path histories. Therefore, the resulting changes in A_0 may not be statistically correlated with the SAR, in agreement with the empirical evidence reported in the above reference.

Despite the above complexity, it is still possible to get some relevant insights from the time records of A_0. In core VC-1 (Fig. 7) A_0 shows a distinct behaviour for mass depths over ~ 4 g cm^{-2}, which according to the chronology correspond to dates before 1920. Lima et al. (2005b) studied the isotopic ratio ^{206}Pb/^{207}Pb in this core. This ratio showed a clear maximum in the mid-1800s, likely linked to the mining and smelting of Pb ores in the Upper Mississippi Valley district. Their findings also suggested that coal could have played a secondary role in Pb emissions after 1920. They concluded: 'The isotopic composition of the most recent portion of the Pettaquamscutt River sediment record is unlikely to be explained by mixing of natural sources, ore smelting, and coal combustion, as was the case for the period between 1735 and 1920' (Lima et al., 2005b). These changes in the provenance of mass flows also left their fingerprints in A_0, as seen in Fig. 7.

Core VC-2 comprises a 42.5-year record. It was sliced at 2-year intervals above the 1950 horizon, and at 5-year intervals below it (Koide et al., 1972). In Fig. 8 A_0 roughly shows a

Preprints (www.preprints.org) | NOT PEER-REVIEWED | Posted: 11 January 2022 doi:10.20944/preprints202201.0143.v1

~10-year rhythm in its half-upper portion, which for the last three decades could be at least partially linked to variability in the annual rainfall. This is shown in Fig. 10. It compares A_0 from varves and from TERESA with the annual rainfall in Santa Barbara (data from Ryan, 1994) after averaging for the same 2 or 5 years intervals than varves. The correlation is statistically significant at 95% confidence level or higher for several simple regression models, the double reciprocal being the best performance (correlation 0.6717; p = 0.012) among the library functions of the Satgraphics Centuriom 18 software. Studying the particular way in which annual rainfall could contribute to modifying A_0 in this aquatic environment (induced changes in provenances, granulometry, etc.) is beyond the scope of the available dataset.

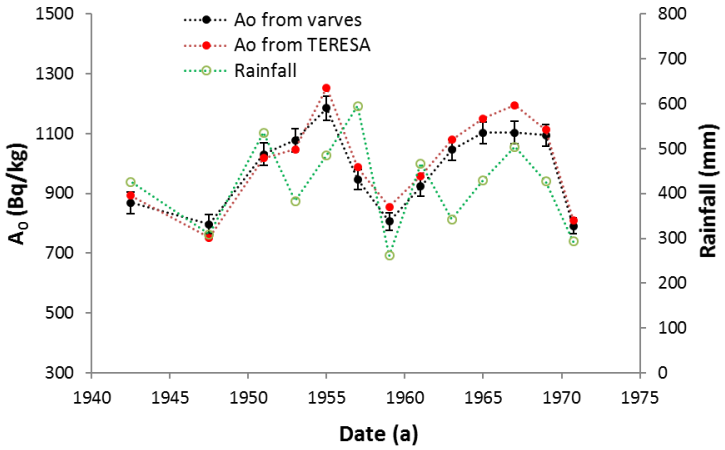

Figure 10. A_0 from varves and TERESA (see Fig. 8) compared against the annual rainfall in Santa Barbara (data from Ryan, 1994) after averaging over the temporal interval of the sediment slicing (2 years after 1950 and 5 years before such date).

In Fig. 9, A_0 for core VC-3 shows three distinct periods of different sedimentation conditions that can be explained by the catchment history, as detailed discussed by Tylmann et al. (2016). Briefly, in 1920 a road was built and it isolated the Lake Zabinskie from the direct influence of the Lake Gołdopiwo waters**.** The new conditions prevailed until ca. 1970, when increasing tourism resulted in the enlargement of the recreation centre located on the northern shore of the lake and in increased eutrophication. The temporal variability of A_0 shows a rich structure, particularly for the intermediate and deeper portions of the core. These changes could be of interpretative interest, but this study goes beyond the possibilities of the available data set.

5. Conclusions

The ^{210}Pb method allows for establishing chronologies at centennial scale in sedimentary deposits. Some of the ^{210}Pb-based models can output historical records of SARs and A_0. The former have been used in the scientific literature to track past changes in the sedimentary conditions. To date, little attention has been paid to A_0.

In addition to propagated errors from the analytical uncertainties, model results are affected by model errors, arising for the partial or null accomplishment of some of their basic assumptions. Synthetic cores are virtual laboratories for assessing model errors, and further support can be found in varved sediments for which an independent chronology is available.

This work has focused on the effects of a random variability of the $^{210}Pb_{exc}$ fluxes in the A_0 and SARs values estimated by the CRS, CS, PLUM and TERESA models.

Preprints (www.preprints.org) | NOT PEER-REVIEWED | Posted: 11 January 2022 doi:10.20944/preprints202201.0143.v1

Independently of the model choice, SARs were largely affected by model errors, resulting in some large and spurious deviations from the true values. This poses into question their general use for tracking past environmental changes.

The initial activity concentrations were less sensitive to model errors and their trends of change with time may reflect real changes in environmental conditions, as has been shown with the study of a set of real cores from varved sediments.

From the assessed models, CRS and TERESA produced the most reliable estimates for the initial activity concentrations.

Annex A

Here we will consider existing ^{210}Pb-based models potentially allowing for the estimation of time series of SARs and/or A_0, namely the CRS, CS, CIC, PLUM, SIT and TERESA models. They share three assumptions: i) continuity of the sequence; ii) $^{210}Pb_{exc}$ behaves as a particle-associated tracer and new inputs are deposited at the SWI over the previously existing material; iii) there is no post-depositional redistribution. Each model adds a particular fourth assumption, allowing for decoding the chronology from the measurements of mass thickness and $^{210}Pb_{exc}$ activity concentrations conducted in a discrete number of sediment slices. The slice-averaged value of the sedimentation rates, initial activity concentrations, and paleofluxes can be derived from direct measurements and the chronology, as shown in Section 2. The model assumptions can allow for alternative but equivalent estimates of the above magnitudes, as shown below. Symbols are used as presented in Section 2.

CRS model

The CRS model adopts the above assumptions i) to iii), and it assumes a constant rate of supply (a constant $^{210}Pb_{exc}$ flux onto the SWI) and a steady state for the total inventory. It works with the $^{210}Pb_{exc}$ inventory below the sediment horizon at mass depth m, Σ_m:

$$\Sigma_m = \int_m^\infty A(m')dm'. \quad \text{(A-1)}$$

The total inventory below SWI, Σ_0, is given by Eq. A-1 for m = 0. Assuming a steady state Σ_0, the age of the sediment horizon at mass depth m is (Appleby and Oldfield, 1978):

$$T(m) = \frac{1}{\lambda}\ln(\frac{\Sigma_0}{\Sigma_m}) \quad \text{(A-2)}$$

The mean SAR value for a sediment slice can be estimated by Eq. 2. An alternative formula has been suggested (e.g., Appleby and Oldfield, 1978), but it needs introducing the additional assumption of steady-state Σ_m, what is equivalent to assume steady-state $A(m)$ profiles. Therefore, a steady state Σ_m requires compensating the advective flow on the horizon m, $wA(m)$, with the radioactive decay below it, $wA(m)$=$\lambda\Sigma_m$, so that

$$w = \frac{\lambda\Sigma_m}{A(m)}. \quad \text{(A-3)}$$

Eq. A-3 also arises as the first-order expansion of Eq. 2 when replacing ΔT by its analytical expression through Eq. A-2 and taking into account that $\Sigma_{m-\Delta m} = \Sigma_m + A(m)\Delta m$. The approach holds for $\frac{A(m)\Delta m}{\Sigma_m} \ll 1$.

The assumption of steady state Σ_0 is mandatory for the model construction, and it relates the radioactive decay of Σ_0 with the constant flux at the SWI: $\phi = \lambda\Sigma_0$. As the flux is assumed to remain constant over time, Eq. 3-4 can be used with the slice-averaged values and the above estimate of w. In this way, it is possible estimating $A'_{0,i}$.

Preprints (www.preprints.org) | NOT PEER-REVIEWED | Posted: 11 January 2022 doi:10.20944/preprints202201.0143.v1

Standard error-propagation equations (Bevington and Robinson, 2003) apply for estimating the propagated uncertainties in $T(m), w$ and A_0. Equation A-3 yields to smaller propagated errors than Eq. 2.

The fundamentals and applications of the piecewise version of the CRS model can be seen, among others, in Appleby (2001) and Abril (2019; 2020). For this and other basic models, including their piecewise versions, readers can find of interest the software *serac*, an R package by Bruel and Sabatier (2020).

PLUM model

The PLUM model is the Bayesian formulation of the 'constant flux' model. It was first presented by Aquino-López et al. (2018), with additional developments in the work by Aquino-López et al. (2020). PLUM does not require a steady-state total inventory, and because of this, it can be applied to cores with incomplete recovery of inventories. The basic equation for the model establishes that the $^{210}Pb_{exc}$ per unit area contained in a sediment slice is the result of the integrated deposition of the constant flux over a certain time interval, after accounting for radioactive decay (as in Eq. 3, but with a constant flux). The authors used the Bacon age depth function that involves accretion and memory parameters. The model uses prior distributions that define a range of values for $^{210}Pb_{exc}$ fluxes, the supported ^{210}Pb fraction, and the memory and accretion parameters. Then PLUM obtains Monte Carlo samples using the t-walk algorithm (Aquino-López et al., 2018). The model output is a cloud of chronological lines from which the values for the median and the 95% confidence interval can be reported.

The CRS model is the natural limit of the PLUM when the constant flux has lasted long enough to achieve a steady-state total inventory. Thus, the use of the PLUM model has been demonstrated against the classical CRS solution for real cases and with synthetic cores generated under the assumption of a constant rate of supply (Aquino-López et al., 2018).

The PyPlum version for Python (https://github.com/maquinolopez/PyPlum) is the full implementation of the PLUM model by Aquino-López et al. (2018), and it has been the one used for the present work.

SIT model

It has been claimed that the SIT model (sediment isotope tomography; Carroll and Lerche, 2003) can handle fluxes and SARs that independently vary with time, under assumptions i) to iii). Nevertheless, it has been shown that this model lacks a sound physical basis; and, particularly, it misuses the Fourier expansion series (Abril, 2015). Consequently, it will not be considered here.

CIC-model

The CIC model adopts the above assumptions i) to iii), and assumes a constant initial activity concentration at the SWI, A_0. Then, the age of the sediment horizon at mass depth *m*, with a measured specific activity concentration $A(m)$, is:

$$t_m = \frac{1}{\lambda}\ln[\frac{A_0}{A(m)}]. \quad \text{(A-4)}$$

As it assumes constant A_0, it could only produce historical records for SARs. A physical scenario with initial activity concentrations and SAR values independently and randomly varying around their respective mean values can be suitable for a CIC model, but the meaningful chronological line is the trend line defined by the CIC ages, which are estimated after stating the value of the initial activity concentration (Abril, 2020). In practice, this implies adopting a single (mean) value for SAR, as in the CF-CS model, otherwise some age-reversals

Preprints (www.preprints.org) | NOT PEER-REVIEWED | Posted: 11 January 2022 doi:10.20944/preprints202201.0143.v1

and negative SARs can occur. Consequently, model errors make the CIC model unusable for reporting historical records of SARs, so it will not be further considered in this study. It should be noted that despite the above limitation, the piecewise version of the CIC model still can provide some gross view of changes in sedimentary conditions (e.g., Abril et al., 2018; Abril 2020).

CS - constant SAR model

Under assumptions i) to iii) with a constant SAR, w, and varying fluxes, time markers (such as ^{137}Cs peaks) can be used to estimate SAR and then to build up a chronology: $t_m = m/w$. As it assumes constant SAR, this model only can produce historical records for initial activity concentrations (after Eq. 7).

TERESA model

The fundamentals of the TERESA model (Time Estimates from Random Entries of Sediments and Activities) and its validation against synthetic cores and real data from varved sediments can be found in the work of Abril (2016), and a multimodal version has been presented in Abril (2020). Further applications can be found in Botwe et al. (2017) and Klubi et al. (2017) for harbour and estuarine sediments, and in Iurian et al. (2021) for saltmarsh sediments; thus, only a brief summary is presented in what follows.

The model adopts the above assumptions i) to iii), and assumes that ^{210}Pb$_{exc}$ fluxes are governed by 'horizontal inputs', so there is a statistical correlation between the fluxes and SAR (Abril and Brunskill, 2014).

For a sediment core that has been sectioned into N slices of mass thickness Δm_i, (i =1, 2,...N), each has an associated age interval, ΔT_i, a mean SAR value w_i, and an associated initial activity concentration $A_{0,i}$ (the one encountered for the sediment slice at the SWI). The TERESA model operates with SARs and initial activities for which slice i adopts the values (w_i, $A_{0,i}$), both varying along the core, but closely following normal distributions around their respective arithmetic mean values, $\bar{w}$ and $\bar{A}_0$, with standard deviations σ_w and σ_A, respectively, being s_w and s_A their typified values (standard deviations divided by mean values). Providing a first estimation of $\bar{w}$, $\bar{A}_0$, s_w and s_A, the model generates independent random distributions for w_i and $A_{0,i}$ by using two randomly sorted sets of N normal-typified $z_{1,i}$ and $z_{2,i}$ values:

$$A_{0,i} = \bar{A}_o(1 + z_{1,i}s_A) \; ; \; w_i = \bar{w}(1 + z_{2,i}s_w) \qquad \text{(A-5)}$$

Furthermore, an algorithm solves their best arrangement downcore to fit the experimental ^{210}Pb$_{exc}$ vs. mass depth profile, generating then solutions for the chronological line and for the histories of SAR and fluxes (Abril, 2016). As the result depends on the first estimation of $\bar{w}$, $\bar{A}_0$, s_w and s_A, the model applies a mapping technique by iterating the whole process for each parameter varying over a wide range. The error function, Q^2, measures the overall quality of the fit for each individual run of the model:

$$Q^2 = \sum_{i=1}^{N} \frac{(A_{th,i} - A_i)^2}{\sigma_i^2} \; ; \quad \chi^2 = Q^2/f; \qquad \text{(A-6)}$$

where A_i and σ_i are, respectively, the measured value and the analytical error of the activity concentration of the slice with index i; $A_{th,i}$ is the corresponding value estimated by the model, and f is the number of degrees of freedom. Parametric maps of the χ-function serve to find the best solution and to support error estimates (Abril, 2016; Bevington and Robinson, 2003). Alternatively, the model's output can be better constrained with time markers, when available. This work uses the stand-alone version of the model with the sorting Method A (Abril, 2016), and its fast-multimodal formulation (FM-TERESA; Abril, 2020).

Preprints (www.preprints.org) | NOT PEER-REVIEWED | Posted: 11 January 2022 doi:10.20944/preprints202201.0143.v1

It should be noted that TERESA does not need the total inventory of $^{210}Pb_{exc}$, but activity measurements must be continuous over the sediment slice sequence.

Although TERESA works with varying w_i and $A_{0,i}$, there are various sources of model errors:

i) TERESA assumes normal distributions for w_i and $A_{0,i}$, while the true ones occurring in each study case can deviate from normality.

ii) Even when real distributions are normal, method A (Abril, 2016) uses a fixed random arrangement of ($z_{1,i}$, $z_{2,i}$) pairs while optimizes the values of of $\overline{w}$, $\bar{A}_0$, s_w and s_A; consequently the model distributions are always a proxy to the true ones. This is improved in the multimodal version of TERESA. Method B for sorting (Abril, 2016) combines each $z_{1,i}$ value with all the possible remaining options for $z_{2,i}$, what increases the computational requirements. It allows for closer solutions for synthetic cores, but its advantages for real cases have not been sufficiently demonstrated.

iii) The primary result of the TERESA model is the chronology, which is linked to the w_i values, while $A_{0,i}$ are used for sorting the pairs ($z_{1,i}$, $z_{2,i}$). The best choice for $A_{0,i}$ is mediated by the initial arrangement of these pairs of data. It will be shown that this produces a good proxy to the true values, but the agreement can be improved by using Eq. 7.

The codes written in Quick-Basic and all the associated files required for TERESA and FM-TERESA are available in the multimedia component of the paper Abril (2020): https://doi.org/10.1016/j.quageo.2019.101032

References

Aalto, R., Nittrouer, C.A., 2012. ^{210}Pb geochronology of flood events in large tropical river systems. Phil. Trans. R. Soc. A 370, 2040‑2074.

Abril, J. M., 1998a. Basic microscopic theory of the distribution, transfer and uptake kinetics of dissolved radionuclides by suspended particulate matter. Part I: theory development. J. Environ. Radioact. 41, 307-324.

Abril, J. M., 1998b. Basic microscopic theory of the distribution, transfer and uptake kinetics of dissolved radionuclides by suspended particulate matter. Part II: applications. J. Environ. Radioact. 41, 325-341.

Abril, J.M., 2003. A new theoretical treatment of compaction and the advective-diffusive processes in sediments. A reviewed basis for radiometric dating models. J. Paleolimnol. 30, 363–370.

Abril, J.M., 2004. Constraints on the use of Cs-137 as a timemarker to support CRS and SIT chronologies. Environ. Pollut. 129, 31–37.

Abril, J.M., 2015. Why would we use the Sediment Isotope Tomography (SIT) model to establish a ^{210}Pb-based chronology in recent-sediment cores? J. Environ. Radioact. 143, 40-46.

Abril, J.M., 2016. A ^{210}Pb-based chronological model for recent sediments with random entries of mass and activities: Model development. J. Environ. Radioact. 151, 64-74.

Abril, J.M., 2019. Radiometric dating of recent sediments: On the performance of ^{210}Pb-based CRS chronologies under varying rates of supply. Quat. Geochronol. 51, 1-14.

Abril, J.M., 2020. Multimodal-TERESA, a ^{210}Pb-based radiometric dating model for recent sediments under largely varying rates of supply. Quat. Geochronol. 55, 101032.

Abril, J.M., Brunskill, G.J., 2014. Evidence that excess ^{210}Pb flux varies with sediment accumulation rate and implications for dating recent sediments. J. Paleolimnol. 52, 121-137.

Abril, J.M., Fraga, E., 1996. Some physical and chemical features of the variability of kd distribution coefficients for radionuclides. J. Environ. Radioact. 30 (3), 253-270.

Abril, J.M., Gharbi, F., 2012. Radiometric dating of recent sediments: beyond the boundary conditions. J. Paleolimnol. 48, 449–460.

Abril, J.M., García-León, M., García-Tenorio, R., Sánchez, C.I., El- Daoushy, F., 1992. Dating of marine sediments by an incomplete mixing model. J. Environ. Radioact. 15, 135–151.

Abril, J.M., San Miguel, E.G., Ruiz-Cánovas, C., Casas-Ruiz, M., Bolívar, J.P., 2018. From floodplain to aquatic sediments: Radiogeochronological fingerprints in a sediment core from the mining impacted Sancho Reservoir (SW Spain). Sci. Total Environ. 631–632, 866-878.

Alonso-Hernández, C.M., Díaz-Asencio, M., Muñoz-Caravaca, A., Delfanti, R., Papucci, C., Ferretti, O., Crovato, C., 2006. Recent changes in sedimentation regime in Cienfuegos Bay, Cuba, as inferred from ^{210}Pb and ^{137}Cs vertical profiles. Cont. Shelf Res. 26,153‑167.

Appleby, P.G., 1998. Dating recent sediments by ^{210}Pb: Problems and solutions. In E. Ilus (Ed.), STUK-A145, Finland; pp. 7-24.

Appleby, P.G., 2001. Chronostratigraphic techniques in recent sediments. In: Last W.L. and Smol J.P. (Eds) Tracking environmental change using lake sediments. Basin analysis, coring, and chronological techniques. Developments in paleoenvironmental research. Kluwer, Dordrecht. pp. 171–203.

Appleby, P.G., Oldfield, F., 1978. The calculation of lead-210 dates assuming a constant rate of supply of unsupported ^{210}Pb to the sediment. Catena 5, 1–8.

Aquino-López, M.A., Blaauw, M., Christen, J.A., Sanderson, N.K., 2018. Bayesian Analysis of ^{210}Pb Dating. J. Agric. Biol. Environ. Stat. 23, 317-333.

Aquino-López, M.A., Ruiz-Fernández, A.C., Blaauw, M., Sanchez-Cabeza, J.A-. 2020. Comparing classical and Bayesian ^{210}Pb dating models in human-impacted aquatic environments. Quat. Geochronol. 60, 101106.

Arias-Ortiz, A., Masqué, P., Garcia-Orellana, J., Serrano, O., Mazarrasa, I., Marbà, N., Lovelock, C.E., Lavery, P.S., Duarte, C.M., 2018, Reviews and syntheses: ^{210}Pb-derived sediment and carbon accumulation rates in vegetated coastal ecosystems: setting the record straight. Biogeoscience Discussions. doi: 10.5194/bg-2018-78.

Barros, H., Abril, J.M., 2004. Experimental and modelling study on the uptake and desorption kinetics of ^{133}Ba by suspended estuarine sediments from southern Spain. Water research 38 (3), 749-755.

Barros, H., Laissaoui, A., Abril, J.M., 2004. Trends of radionuclide sorption by estuarine sediments. Experimental studies using ^{133}Ba as a tracer. Sci. Total Environ. 319 (1-3), 253-267.

Begy, R.-Cs, Simon, H., Kelemen, Sz., Preoteasa, L., 2018. Investigation of sedimentation rates and sediment dynamics in Danube Delta lake system (Romania) by ^{210}Pb dating method. J. Environ. Radioact. 192, 95-104. https://doi.org/10.1016/j.jenvrad.2018.06.010

Bevington, P. A., Robinson, D.K., 2003. Data Reduction and Error Analysis for the Physical Sciences, 3rd Edition. McGraw-Hill, New York.

Botwe, B.O., Abril, J.M., Schirone, A., Barsanti, M., Delbono, I., Delfanti, R., Nyarko, E., Lens, P.N.L., 2017. Settling fluxes and sediment accumulation rates by the combined use of sediment traps and sediment cores in Tema Harbour (Ghana). Sci. Tot. Environ. 609, 1114-1125.

Bruel, R., Sabatier, P., 2020. *serac*: an R package for ShortlivEd RAdionuclide chronology of recent sediment cores. J. Environ. Radioact. 225, 106449. https://doi.org/10.1016/j.jenvrad.2020.106449

Carroll, J., Lerche, I., 2003. Sedimentary Processes: Quantification Using Radionuclides. Elsevier, Oxford.

Chen, X., Qiao, Q., McGowan, S., Zeng. L., Stevenson, M.A., Xu, L., Huang, Ch., Liang, J., Cao, Y., 2019. Determination of geochronology and sedimentation rates of shallow lakes in the middle Yangtze reaches using ^{210}Pb, ^{137}Cs and spheroidal carbonaceous particles. Catena 174, 546–556. https://doi.org/10.1016/j.catena.2018.11.041

El Mrabet, R., Abril, J.M., G Manjón, G., García-Tenorio, R., 2001. Experimental and modelling study of plutonium uptake by suspended matter in aquatic environments from southern Spain. Water Research 35 (17), 4184-4190.

Goldberg, E.D., 1963. Geochronology with Pb-210. Proceedings of a Symposium of Radioactive Dating, International Atomic Energy Agency, Vienna. pp. 121–131.

He, Q., Walling, D., 1996. Interpreting particle size effects in the adsorption of ^{137}Cs and unsupported ^{210}Pb by mineral soils and sediments. J. Environ. Radioact. 30(2), 117-137.

Iurian, A.R., Millward, G.E., Blake, W., Abril Hernández, J.M., 2021. Fine-tuning of ^{210}Pb-based methods for dating vegetated saltmarsh sediments. Quat. Geochronol. 62, 101153. https://doi.org/10.1016/j.quageo.2021.101153

Klubi, E., Abril, J.M., Nyarko, E., Laissaoui, A., Benmansour, M., 2017. Radioecological assessment and radiometric dating of sediment cores from dynamic sedimentary systems of Pra and Volta estuaries (Ghana) along the Equatorial Atlantic. J. Environ. Radioact. 178-179,116-126.

Koide, M., Soutar, A., Goldberg, E.D., 1972. Marine geochronology with ^{210}Pb. Earth Planet. Sci. Lett. 14, 442–446.

Koide, M., Bruland, K., Goldberg, E.D., 1973. Th-228/Th-232 and Pb-210 geochronologies in marine and lake sediments. Geochim. Cosmochim. Acta 37, 1171–1187.

Krishnaswamy, S., Lal, D., Martin,,J.M., Meybek, M., 1971. Geochronology of lake sediments. Earth Planet. Sci. Lett. 11, 407–414.

Laissaoui, A., Benmansour, M., Ziad, N., Ibn Majah, M., Abril, J.M., Mulsow, S. 2008. Anthropogenic radionuclides in the water column and a sediment core from the Alboran Sea: application to radiometric dating and reconstruction of historical water column radionuclide concentration. J. Paleolimnol. 40, 823–833

Lima, A.L., Hubeny, J.B., Reddy, C.M., King, J.W., Hughen, K.A., Eglinton, T.I., 2005a. High resolution historical records from Pettaquamscutt River basin sediments: 1. ^{210}Pb and varve chronologies validate record of ^{137}Cs released by the Chernobyl accident. Geochim. Cosmochim. Acta 69, 1803–1812.

Lima, A.L., Bergquist, B.A., Boyle, E.A., Reuer, M.K., Dudas, F.O., Reddy, C.M., Eglinton, T.I., 2005b. High-resolution historical records from Pettaquamscutt River basin sediments: 2. Pb isotopes reveal a potential new stratigraphic marker. Geochim. Cosmochim. Acta 69 (7), 1813–1824.

Lu, X., Matsumoto, E., 2005; Recent sedimentation rates derived from ^{210}Pb and ^{137}Cs methods in Ise Bay, Japan. Estuar. Coast. Shelf Sci. 65, 83-93.

Mabit, L., Benmansour, M., Abril, J.M., Walling, D.E., Meusburger, K., Iurian, A.R., Bernard, C., Tarjan, S., Owens, P.N., Blake, W.H., Alewell, C., 2014. Fallout ^{210}Pb as a soil and sediment tracer in catchment sediment budget investigations: a review. Earth Sci. Rev. 138, 335-351.

Madsen, A.T., Murray, A.S., Andersen, T.J., Pejrup M., 2007. Temporal changes of accretion rates on an estuarine salt marsh during the late Holocene — Reflection of local sea level changes? The Wadden Sea, Denmark. Mar. Geol. 242, 221–233.

Mantero, J., Abril-Hernández, J.M., Garcia-Tenorio, R., Klubi, E., Nyarko, E., 2019. Experimental study on the use of granulometric speciation for the radiometric dating of recent sediments. J. Environ. Radioact. 208‑209, 106016. https://doi.org/10.1016/j.jenvrad.2019.106016

Robbins, J.A., 1978. Geochemical and Geophysical applications of radioactive lead isotopes. In: Nriago JP (ed) Biochemistry of Lead in the Environment. Elsevier, Amsterdam, pp 285-393

Robbins, J.A., Edgington, D.N., 1975. Determination of recent sedimentation rates in Lake Michigan using ^{210}Pb and ^{137}Cs. Geochim. Cosmochim. Acta 39, 285–304.

Ryan, G., 1994. Climate of Santa Barbara, California. NOAA Technical Memorandum NWS WR-225.

Sánchez-Cabeza, J.A., Ruíz-Fernández, A.C., 2012. ^{210}Pb sediment radiochronology: an integrated formulation and classification of dating models. Geochim. Cosmochim. Acta 82, 183-200.

Smith, J.N., 2001. Why should we believe ^{210}Pb sediment geochronologies? J. Environ. Radioact. 55(2), 121-123.

Sun, X., Fan, D., Tian, Y., Zheng, S., 2018. Normalization of excess ^{210}Pb with grain size in the sediment cores from the Yangtze River Estuary and adjacent areas: implications for sedimentary processes. Holocene 28 (4), 545‑557.

Trabelsi, Y., Gharbi, F., El Ghali, A., Oueslati, M., Samaali, M., Abdelli, W., Baccouche, S., Ben Tekaya, M., Benmansour, M., Mabit, L., Ben M'Barek, N., Reguigui, N., Abril, J.M., 2012. Recent sedimentation rates in Garaet El Ichkeul Lake, NW Tunisia, as affected by the construction of dams and a regulatory sluice. J. Soils Sediments 12, 784–796. https://doi.org/10.1007/s11368-012-0496-y

Tylmann, W., Bonk, A., Goslar, T., Wulf, S., Grosjean, M., 2016. Calibrating ^{210}Pb dating results with varve chronology and independent chronostratigraphic markers: Problems and implications. Quat. Geochronol. 32, 1-10.

Zaborska, A., Carroll, J., Papucci, C., Pempkowiak, J., 2007. Intercomparison of alpha and gamma spectrometry techniques used in ^{210}Pb geochronology. J. Environ. Radioact. 93, 38-50.